Free Radical Research

ISSN: 1071-5762 (Print) 1029-2470 (Online) Journal homepage: www.tandfonline.com/journals/ifra20

Amelioration of late-onset hepatic steatosis in *IDH2*-deficient mice

Su Jeong Lee, Hanvit Cha, Hyunjin Kim, Jin Hyup Lee & Jeen-Woo Park

To cite this article: Su Jeong Lee, Hanvit Cha, Hyunjin Kim, Jin Hyup Lee & Jeen-Woo Park (2017) Amelioration of late-onset hepatic steatosis in *IDH2*-deficient mice, Free Radical Research, 51:4, 368-374, DOI: 10.1080/10715762.2017.1320554

To link to this article: https://doi.org/10.1080/10715762.2017.1320554

Published online: 05 May 2017.

FREE RADICAL RESEARCH, 2017
VOL. 51, NO. 4, 368–374
https://doi.org/10.1080/10715762.2017.1320554

Taylor & Francis
Taylor & Francis Group

ORIGINAL ARTICLE

Amelioration of late-onset hepatic steatosis in *IDH2*-deficient mice

Su Jeong Lee[a], Hanvit Cha[a], Hyunjin Kim[a], Jin Hyup Lee[b] and Jeen-Woo Park[a]

[a]School of Life Sciences, BK21 Plus KNU Creative BioResearch Group, College of Natural Sciences, Kyungpook National University, Taegu, Republic of Korea; [b]Department of Food and Biotechnology, Korea University, Sejong, Republic of Korea

ABSTRACT

Nonalcoholic fatty liver disease (NAFLD) has a high prevalence in the general population and can evolve into nonalcoholic steatohepatosis (NASH), cirrhosis, and complications such as liver failure and hepatocellular carcinoma. Recently, we reported that mitochondrial $NADP^+$-dependent isocitrate dehydrogenase, encoded by the *IDH2*, plays an important role in the regulation of redox balance and oxidative stress levels, which are tightly associated with intermediary metabolism and energy production. In the present study, we showed that in mice targeted disruption of *IDH2* attenuates age-associated hepatic steatosis by the activation of p38/cJun NH2-terminal kinase (JNK) and p53, presumably induced by the elevation of mitochondrial reactive oxygen species (ROS), which in turn resulted in the suppression of hepatic lipogenesis and inflammation via the upregulation of fibroblast growth factor 21 (FGF21) and the inhibition of NFκB signaling pathways. Our finding uncovers a new mechanism involved in hepatocellular steatosis and IDH2 may be a valuable therapeutic target for the management of NAFLD.

ARTICLE HISTORY
Received 2 February 2017
Revised 26 March 2017
Accepted 14 April 2017

KEYWORDS
IDH2; hepatosteatosis; mitochondrial ROS; FGF21

Introduction

Nonalcoholic fatty liver disease (NAFLD), acknowledged as an important public health problem because of its high prevalence, is considered to be an integral part of the metabolic syndrome that is associated with obesity, hyperlipidemia, and diabetes [1,2]. A chronic imbalance between triglyceride acquisition and its utilization leads to the abnormal accumulation of lipids in the liver, resulting into fatty liver or hepatic steatosis [3]. Although hepatic steatosis itself is benign, the excess triglyceride could result in nonalcoholic steatohepatosis (NASH) [4]. NASH is characterized by inflammation and cellular injury or even death of hepatocytes, and it highly increases the risk of hepatocellular carcinoma and fibrosis of the liver [5].

Mitochondria are the main organelles involved in the production of reactive oxygen species (ROS), and therefore are also the main targets of ROS-induced damage [6,7]. Numerous studies suggest that mitochondrial ROS have evolved as key mediators of communication between the mitochondria and cell for regulation of homeostasis as well as the maintenance of normal cellular functions [8]. We demonstrated that mitochondrial $NADP^+$-dependent isocitrate dehydrogenase (IDH2) is critical for maintaining the cellular redox environment via its ability to generate NADPH by catalyzing the oxidative decarboxylation of isocitrate into α-ketoglutarate [9]. NADPH serves as an essential reducing equivalent needed for recycling the oxidized form of glutathione (GSH) in mitochondria and is required for the mitochondrial antioxidant defense systems including the NADPH-dependent thioredoxin system [10,11].

Previously, we reported that *IDH2*-deficient mice, which are resistant to age-associated diet-induced obesity, exhibit several metabolic changes related to glucose tolerance and insulin sensitivity as well as promotion of energy expenditure via increase of thermogenesis [12]. We proposed that IDH2 plays a role as the central regulator of adipocyte lipid metabolism and energy expenditure, thereby directly combating obesity and obesity-related insulin resistance. Here, we show that mice with targeted disruption of *IDH2* attenuate age-associated hepatic steatosis. This function of IDH2 is linked to its capacity to suppress lipogenesis and inflammation through mitochondrial ROS-dependent activation of p38/c-Jun NH2-terminal kinase (JNK) and p53. Our finding uncovers a new mechanism involved in hepatocellular steatosis and suggests that IDH2 could be a valuable therapeutic target for the management of NAFLD.

CONTACT Jeen-Woo Park parkjw@knu.ac.kr School of Life Sciences and Biotechnology, College of Natural Sciences, Kyungpook National University, Taegu, South Korea; Jin Hyup Lee jinhyuplee@korea.ac.kr Department of Food and Biotechnology, Korea University, Sejong, South Korea

Materials and methods

Animal care

Age-matched male *IDH2* knockout (*IDH2*$^{-/-}$) and their littermate wild type (*IDH2*$^{+/+}$) mice with C57BL/6 genetic background were used in this study [13]. The animals were housed in climate-controlled, specific pathogen-free barrier facilities under a 12-h light-dark cycle, and chow and water were provided *ad libitum*. The Institutional Animal Care and Use Committee at the Kyungpook National University approved the experimental protocols for this study. Mice were fed a normal chow diet (12% fat calories, Purina Laboratory Rodent Diets 38057).

Histological analysis

Tissues were harvested, fixed in 4% (w/v) paraformaldehyde in phosphate-buffered saline (PBS), and embedded in paraffin. Then, 5-μm-thick tissue sections were deparaffinized, rehydrated, and used for staining, immunohistochemistry, and immunofluorescence. For antigen retrieval, the slides were submerged in 10 mM sodium citrate (pH 6.0) and heated to 90 °C for 20 min. Tissue lipid content was assessed by 4,4-difluoro-1,3,5,7,8-pentamethyl-4-bora-3a,4a-diaza-*s*-Indacene (BODIPY) staining of paraffin-embedded tissue sections. Cryosectioned tissues (3 μm thick) were fixed with 1% formalin for 10 min, and stained with BODIPY (Molecular Probes, Carlsbad, CA) working solution, stocked in ethanol (2 mg/ml) after diluting to 1000× with PBS, for 30 min. The sectioned tissues were then counterstained with 4,6-diamidino-2-phenylindole (DAPI) and mounted. Immunohistochemistry was performed using a VECTASTAIN ABC Kit (PK-4001, Vector Laboratories, Burlingame, CA), according to the manufacturer's instructions, using antibody against 4-hydroxynonenal (4-HNE) and sterol regulatory element-binding protein1 (SREBP1) (Santa Cruz Biotechnology, Santa Cruz, CA), acetyl-CoA carboxylase (ACC), and fatty acid synthase (FAS) (Cell Signaling Technology, Beverly, MA). Antibodies used for immunofluorescence staining were anti-Opa1 (BD Biosciences, Franklin Lake, NJ), anti-Mfn1, and anti-Fis1 (Sigma Aldrich, St. Louis, MO). Images were acquired using a light microscope (Nikon Eclipse 80i) or confocal microscope (Nikon E600).

Immunoblot analysis

Antibodies were from the following sources: Prx-SO_3 (Abcam), SREBP1; actin (Santa Cruz Biotechnology, Santa Cruz, CA); ACC, FAS, C/EBPα, C/EBPβ, p-p38, p38, JNK, fibroblast growth factor 21(FGF21), Akt, pAkt, Erk, pErk, IKKα, IKKβ, pIKKα/β, pIKBα, NFκB, tumor necrosis factor alpha (TNF-α), and p53 (Cell Signaling Technology, Beverly, MA). Total-protein extracts were separated by 10% SDS-PAGE, and the proteins were transferred to nitrocellulose membranes. The membranes were incubated with the appropriate primary antibodies, washed, and incubated with a horseradish peroxidase-labeled anti-rabbit IgG secondary antibody. Antibody binding was detected with an enhanced chemiluminescence detection kit (Amersham Pharmacia Biotech; Buckinghamshire, UK).

Reverse transcription-polymerase chain reaction (RT-PCR)

RNA was isolated using an RNeasy kit (Qiagen; Hilden, Germany) according to the manufacturer's instructions. RNA (3 μg) used for RT-PCR was extracted using TRIzol reagent and cDNA was synthesized using the Super Scripts First-Strand kit (Invitrogen; Carlsbad, CA) according to the manufacturer's protocol. The sequences of primers used were as follows: *GAPDH*, forward 5′-CGACAGTGTTTCCTCGTCAA-3′, reverse 5′-CCTTTT GGCTCCACCCTTCA-3′; *IDH2*, forward 5′-ATCAAGGAG AAGCTCATCCTGC-3′, reverse 5′-TCTGTGGCCTTGTACT GGTCG-3′. *GAPDH* was used as an internal control. The PCR products were separated on 2% agarose gels and bands were visualized with ethidium bromide staining.

Mitochondrial redox status

In order to determine the levels of mitochondrial ROS, dihydrorhodamine 123 (DHR 123; 2 mg/kg body weight) was administered intraperitoneally, after which the tissues were homogenized and lysed in TEGN buffer. The fluorescence intensity was analyzed using a Shimadzu UV1650 spectrophotometer using excitation and emission wavelengths of 500 and 536 nms, respectively. NADPH concentrations were measured using an enzymatic cycling method, as previously described [12], and were expressed as the ratio of NADPH to total NADP. Mitochondrial and cytosolic fractions were obtained from homogenized liver using differential centrifugation, and the ratio of glutathione disulfide (GSSG)/total glutathione (GSHt) in each fraction was determined. The concentration of GSHt was determined by the rate of formation of 5-thio-2-nitrobenzoicacid at 412 nm ($\varepsilon = 1.36 \times 10^4\,M^{-1}cm^{-1}$), as previously described [12], while GSSG levels were measured using a DTNB-GSSG reductase recycling assay.

Statistical analysis

Results were expressed as mean ± SD. Statistical analysis was performed using Student's *t*-test, and one-way analysis of variance was done for a comparison between the two groups. p Values <0.05 were considered statistically significant.

Results and discussion

Previously, we demonstrated that 10-month-old *IDH2*$^{-/-}$ mice exhibited a marked reduction in body weight compared with wild-type mice and this difference resulted from the lowered adipocyte hypertrophy. However, there had been no significant difference in the body weight from birth to 24 weeks between the two genotypes [12]. To confirm the IDH2 deficiency in the knockout mice used in the present study, we measured the expression of hepatic *IDH2* gene products. As expected, neither *IDH2* mRNA nor the expression of the 47-kDa IDH2 protein was detected by RT-PCR analysis (Figure 1(A)) and immunoblotting analysis (Figure 1(B)), respectively, in the liver tissues harvested from 10-month-old *IDH2*$^{-/-}$ mice.

The hallmark feature of NAFLD is the accumulation of lipids in the form of neutral lipid droplets in hepatocytes [14]. Histological examination of liver tissue from *IDH2*$^{-/-}$ mice with BODIPY (a highly lipophilic bright green dye to evaluate intracellular lipids) staining revealed a reduction in the lipid droplets compared to that in the wild-type mice (Figure 1(C)), indicating

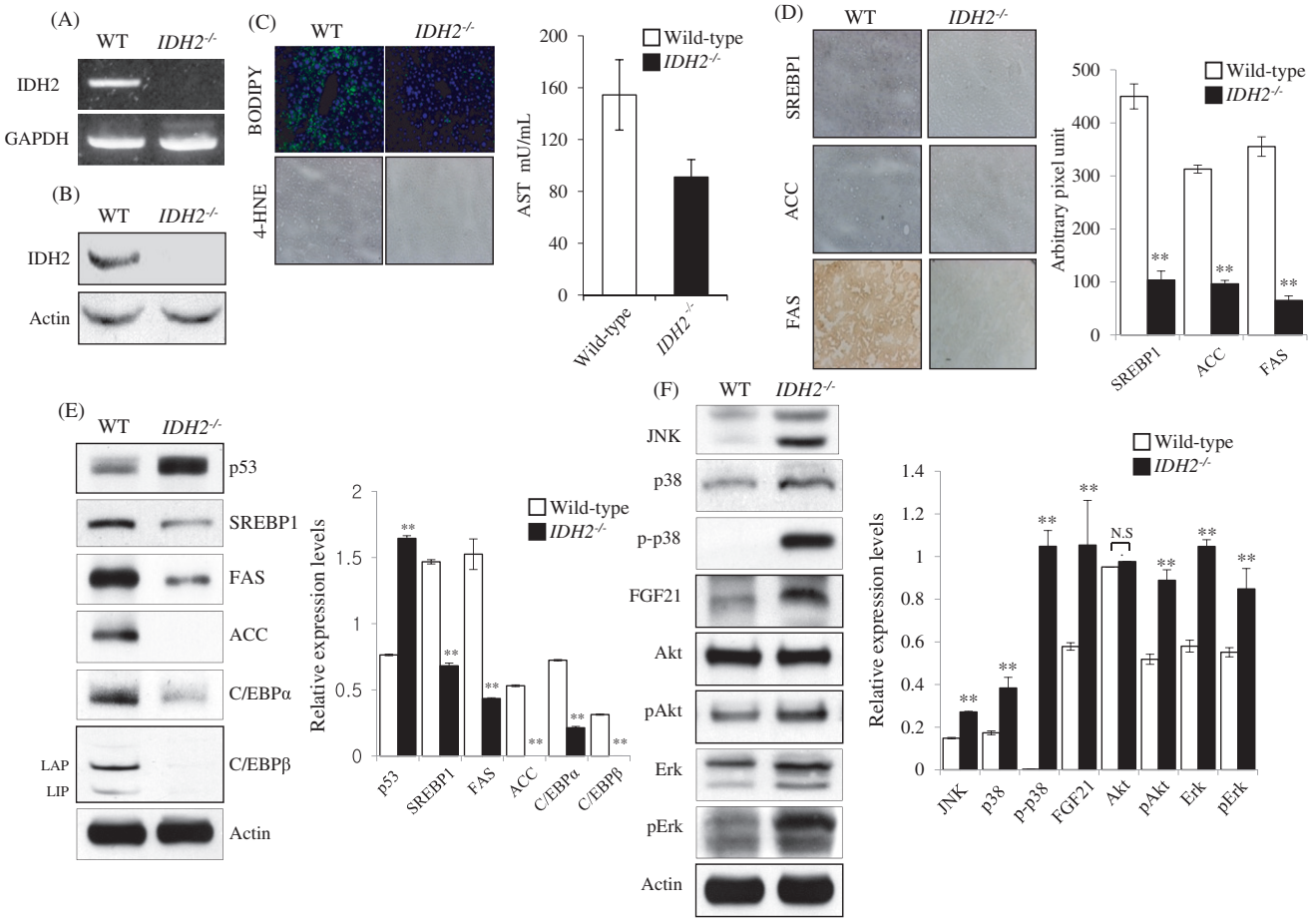

Figure 1. Suppressed hepatic lipogenesis in *IDH2*$^{-/-}$ mice. (A) RT-PCR analysis of gene expression in the liver tissues of wild-type and *IDH2*$^{-/-}$ mice. GAPDH was used as an internal control. (B) Expression levels of IDH2 protein were measured by immunoblotting using anti-IDH2 antibody. Actin was used as a loading control. (C) Representative BODIPY-stained and 4-HNE-stained sections from the livers of wild-type and *IDH2*$^{-/-}$ mice. Activities of serum aspartate transaminase (AST) were measured by Abnova assay kit. Each value represents the mean ± SD from five to six independent experiments. (D) Immunohistochemical staining of proteins related to lipogenesis in the liver of wild-type and *IDH2*$^{-/-}$ mice. (E) Immunoblot analysis of p53 levels and lipogenic protein expression in the liver of wild-type and *IDH2*$^{-/-}$ mice. Actin was used as a loading control. (F) Immunoblot analysis for protein expression of FGF21 and p38 MAPK activation in the liver tissues of wild-type and *IDH2*$^{-/-}$ mice. The figure shows representative data for five to six independent experiments. The protein levels were normalized to the actin levels in the analysis of immunoblotting data. Each value represents the mean ± SD from five to six independent experiments. $^{**}p < 0.01$, between the two genotypes indicated.

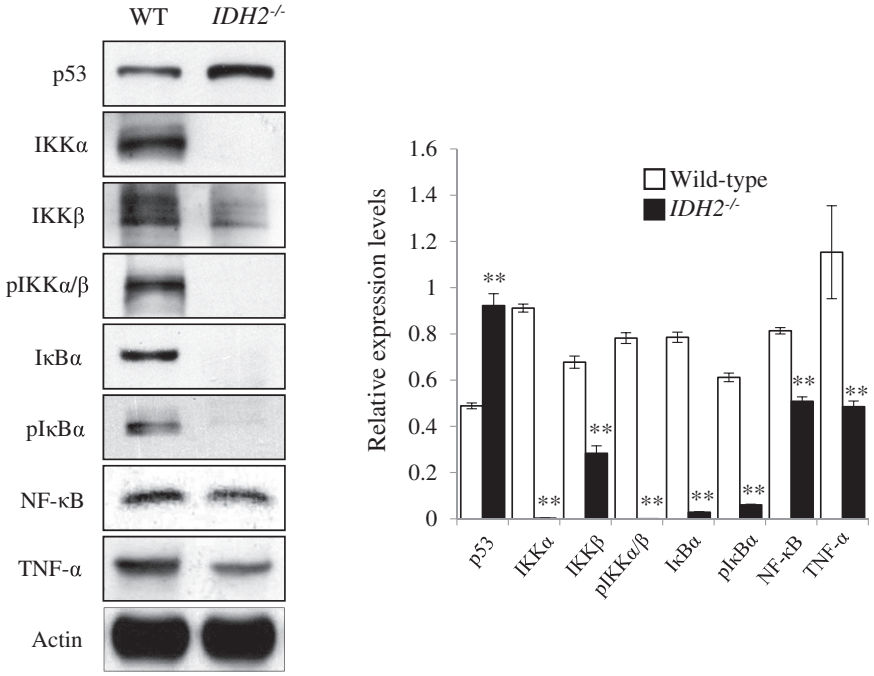

Figure 2. Attenuated hepatic inflammation in *IDH2*$^{-/-}$ mice. Immunoblot analysis of p53 levels and proteins associated with NFκB signaling pathway in the liver of wild-type and *IDH2*$^{-/-}$ mice. Actin was used as a loading control. The protein levels were normalized to the actin level. Each value represents the mean ± SD from five to six independent experiments. $^{**}p < 0.01$, between the two genotypes indicated.

amelioration of late-onset hepatosteatosis in *IDH2*$^{-/-}$ mice. Consistent with the reduced lipid deposition in the liver, the level of 4-HNE, a major lipid peroxidation product, was found to have markedly decreased in *IDH2*$^{-/-}$ mice (Figure 1(C)). In addition, the serum level of aspartate transaminase (AST) (Abnova assay kit) was lower in *IDH2*$^{-/-}$ mice compared with *IDH2*$^{+/+}$ mice (Figure 1(C)). In order to elucidate the molecular basis of these metabolic changes in the liver of *IDH2*$^{-/-}$ mice, we evaluated the expression of lipogenesis-related genes. A key transcriptional regulator of triglyceride synthesis, SREBP1, controls the transcription and expression of lipogenic enzymes such as that of FAS, which catalyzes the first committed step in lipogenesis, and of ACC, which is the rate-limiting enzyme in fatty acid synthesis [15]. We found that the expressions of SREBP1 and its target genes—FAS and ACC—are significantly attenuated in the liver of *IDH2*$^{-/-}$ mice compared with that of the WT mice (Figure 1(D)). The tumor suppressor protein p53 is considered to be a redox active transcription factor that organizes and directs cellular responses against a variety of insults to genomic instability [16,17]. p53 has been demonstrated to regulate key transcription factors responsible for the expression of genes involved in determining cellular lipogenic status such as that of SREBP1 [18]. ACC is activated by CCAAT/enhancer-binding protein α (C/EBPα) and CCAAT/enhancer-binding protein β (C/EBPβ), as well as SREBP1 [19]. C/EBP is originally isolated from rat liver, which plays a critical role in energy metabolism, particularly in the synthesis and mobilization of glycogen and fat [20]. Immunoblotting analysis confirms the upregulation of p53 and downregulation of SREBP1, C/EBP, FAS, and ACC in the liver of *IDH2*$^{-/-}$ mice (Figure 1(E)).

Fibroblast growth factor 21 (FGF21) appears to be primarily produced by the liver and is thought to act on its target tissues, including liver and adipose tissues [21]. FGF21 is a novel hormone that has profound effects on metabolic parameters such as glucose and lipid homeostasis. Furthermore, the hormone has the critical role to promote rapid body weight loss [22]. Recent studies demonstrated that the activation of FGF21 contribute to the reversal of simple fatty liver and NASH through the direct regulation of lipid metabolism and reduced accumulation of hepatic lipids [23]. In addition, MAPK and JNK are established regulators of hepatic metabolism [24,25]. Recent studies demonstrated that regulation of FGF21 expression is attributed to the mediators of p38-MAPK and/or JNK signaling in liver [26]. According to several reports, FGF21 is a target of the hepatic JNK signaling pathway, which is also regulated by the activation of p38 MAPK-mediated mechanism [27]. Expression of FGF21 improves activation of extracellular signal-related kinase (ERK) and Akt signaling pathways [28]. These, Erk and Akt, are related

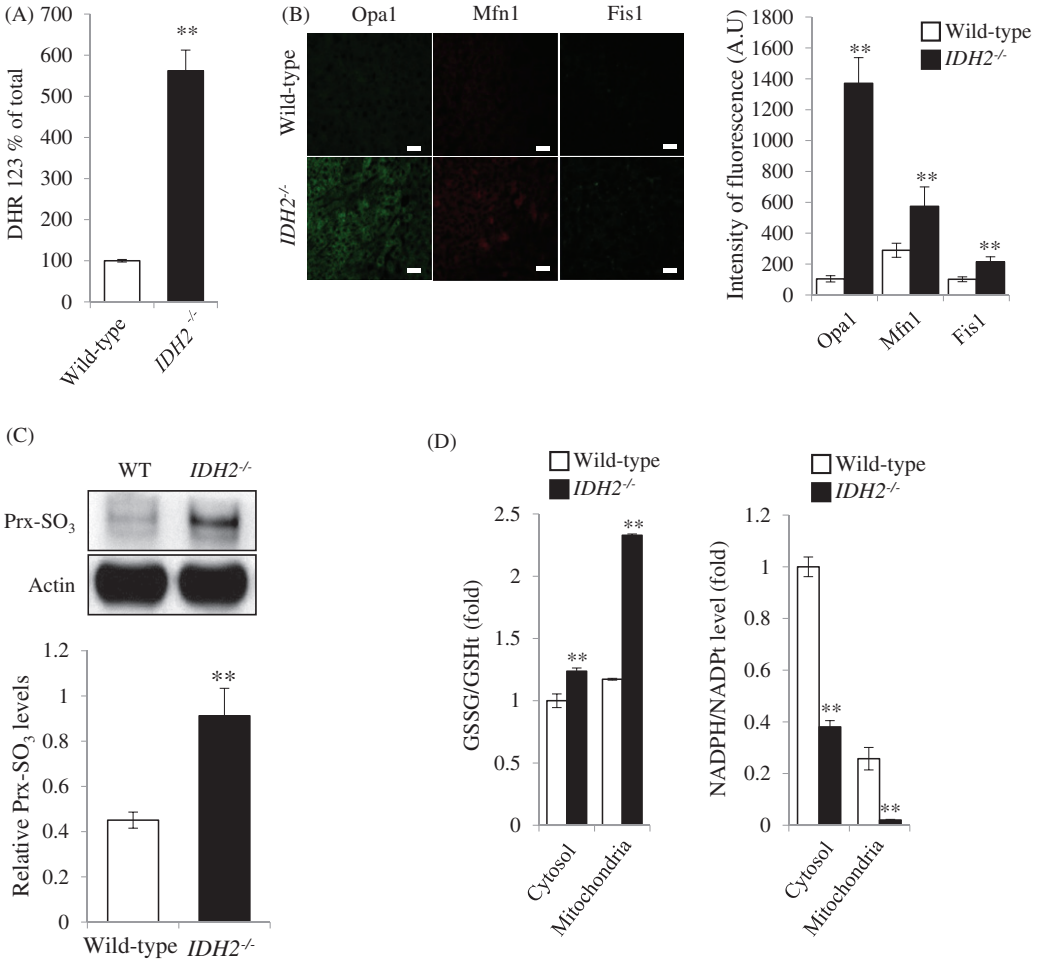

Figure 3. Modulation of hepatic mitochondrial redox status in *IDH2*$^{-/-}$ mice. (A) Quantification of DHR 123 fluorescence level for evaluation of the mitochondrial ROS generation in the liver of wild-type and *IDH2*$^{-/-}$ mice. (B) Immunofluorescence staining of mitochondrial fusion markers Opa1/Mfn1 and a fission marker Fis1 in the liver of wild-type and *IDH2*$^{-/-}$ mice. Histograms represent the quantification of fluorescence intensity. (C) Ratio of GSSG versus total GSH concentration and the ratio of NADPH versus total NADP concentration were measured in the liver tissues of wild-type and *IDH2*$^{-/-}$ mice. Values are presented as the fold change over the levels observed in wild-type mice. Each value represents the mean ± SD from five to six independent experiments. $^{**}p < 0.01$, between the two genotypes indicated. (D) Immunoblot analysis of oxidized peroxiredoxin (Prx-SO_3) level, a marker for intracellular ROS formation in the liver of wild-type and *IDH2*$^{-/-}$ mice. Actin was used as a loading control. The protein levels were normalized to the actin levels.

to the suppression of lipogenesis and fat accumulation in liver [29]. As shown in Figure 1(F), activation of MAPK and upregulation of FGF21 expression supports the alteration of hepatic steatosis via decreased fatty acid synthesis in IDH2 knockout mice. Taken together, we propose that the ROS-mediated activation of p38/JNK-FGF21 axis may be responsible for the suppression of lipogenesis in *IDH2*$^{-/-}$ mice.

Inflammation is a key variable in the progression of hepatic steatosis [30]. Several studies have shown that the tumor suppressor p53 restricts the activation of proinflammatory transcription factor nuclear factor kappa B (NFκB) signaling pathway [31]. Previous studies have identified NFκB and JNK as key regulators of early hepatic inflammatory recruitment and liver injury in NASH [32]. Under basal conditions, NFκB exists as a complex with its inhibitor IκB in the cytoplasm. Upon activation of upstream inflammatory pathways, IκB is phosphorylated by the IκB kinase (IKK) complex, ubiquitinated, and later degraded. This transformation allows NFκB to translocate into the nucleus where it acts as a transcriptional regulator inducing the generation of proinflammatory cytokines. Especially, NFκB activates TNF-α responsible for the progression of metabolic inflammation [33,34]. TNF-α triggers the diverse hepatic lesions of NASH by inducing hepatic inflammation and fibrosis that eventually lead to end-stage liver disease [35]. As expected, the upregulation of p53 leads to the inhibition of NFκB pathway as well as downregulation of TNF-α in the hepatocytes of *IDH2*$^{-/-}$ mice (Figure 2).

Several previous studies have suggested that ROS initiates cellular damage. A plethora of recent studies,

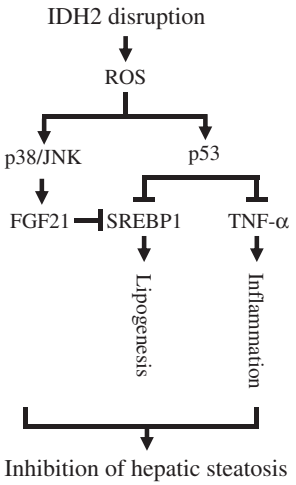

Figure 4. Model for the amelioration of late-onset hepatic steatosis in *IDH2*-deficient mice.

however, have proposed that at physiological levels, ROS can also serve as signaling molecules to regulate normal physiological processes such as oxygen sensing [36]. Furthermore, over the last decade, our knowledge of ROS has become more complex; several reports have suggested that the type and compartmentalization of ROS are likely to regulate distinct biological outcomes [37]. In order to examine the effect of IDH2 deficiency on the redox status of hepatic mitochondria and the subsequent cellular ROS production, we analyzed the mitochondrial ROS by DHR123 (Figure 3(A)), biogenesis (Figure 3(B)) in the hepatocytes of $IDH2^{-/-}$ mice and wild-type mice. We also determined the mitochondrial redox status reflected by the efficiency of GSH recycling and NADPH pool in the tissues from both the genotypes (Figure 3(C)). The data reveal that IDH2 deficiency leads to elevated levels of mitochondrial ROS and the upregulation of mitochondrial biogenesis as well as the shift of mitochondrial redox status to the oxidative state. In addition, the level of peroxiredoxin (Prx)-SO_3, a marker for oxidative damage to the antioxidant enzyme Prx, was also found to have increased in the liver tissue of $IDH2^{-/-}$ mice compared to that of $IDH2^{+/+}$ mice (Figure 3(D)).

The findings of this study summarized in Figure 4 are as follows: (a) The inhibition of IDH2 results in elevated levels of mitochondrial ROS, which leads to the activation of p38/JNK and p53. (b) Activated p38/JNK induces inhibition of lipogenesis-related genes via the upregulation of FGF21. (c) Upregulation of p53 also attenuates lipogenesis-related genes and suppression of inflammation through the inhibition of NFκB pathway. In summary, we provide the first evidence that targeted disruption of *IDH2* attenuates late-onset hepatic steatosis. Therefore, IDH2 is a potential target for the development of pharmacological interventions counteracting hepatic steatosis and related metabolic diseases.

Acknowledgements

This work was supported by the National Research Foundation of Korea (NRF) grants funded by the Korea Government (MSIP) [NRF-2016R1A2B1006280 and NRF-2015R1A4A1042271].

Disclosure statement

No potential conflict of interest was reported by the authors.

Funding

This work was supported by the National Research Foundation of Korea (NRF) grants funded by the Korea Government (MSIP) [NRF-2016R1A2B1006280 and NRF-2015R1A4A1042271].

References

1. Tilg H, Hotamisligil GS. Nonalcoholic fatty liver disease: cytokine-adipokine interplay and regulation of insulin resistance. Gastroenterology 2006;131:934–945.
2. Kirpich IA, McClain CJ. Probiotics in the treatment of the liver diseases. J Am Coll Nutr 2012;31:14–23.
3. Cohen JC, Horton JD, Hobbs HH. Human fatty liver disease: old questions and new insights. Science 2011;332:1519–1523.
4. Wei Y, Clark SE, Thyfault JP, Uptergrove GM, Li W, Whaley-Connell AT, et al. Oxidative stress-mediated mitochondrial dysfunction contributes to angiotensin II-induced nonalcoholic fatty liver disease in transgenic Ren2 rats. Am J Pathol 2009;174:1329–1337.
5. Adams LA, Angulo P, Lindor KD. Nonalcoholic fatty liver disease. CMAJ 2005;172:899–905.
6. Balaban RS, Nemoto S, Finkel T. Mitochondria, oxidants, and aging. Cell 2005;120:483–495.
7. Chan DC. Fusion and fission: interlinked processes critical for mitochondrial health. Annu Rev Genet 2012;46:265–287.
8. Sena LA, Chandel NS. Physiological roles of mitochondrial reactive oxygen species. Mol Cell 2012;48:158–167.
9. Jo SH, Son MK, Koh HJ, Lee SM, Song IH, Kim YO, et al. Control of mitochondrial redox balance and cellular defense against oxidative damage by mitochondrial $NADP^+$-dependent isocitrate dehydrogenase. J Biol Chem 2001;276:16168–16176.
10. Kirsch M, de Groot H. NAD(P)H, a directly operating antioxidant?. FASEB J 2001;15:1569–1574.
11. Nakamura H. Thioredoxin and its related molecules: update 2005. Antioxid Redox Signal 2005;7:823–828.
12. Lee SJ, Kim SH, Park KM, Lee JH, Park J-W. Increased obesity resistance and insulin sensitivity in mice lacking the isocitrate dehydrogenase 2 gene. Free Radic Biol Med 2016;99:179–188.

13. Ku HJ, Ahn Y, Lee JH, Park KM, Park J-W. IDH2 deficiency promotes mitochondrial dysfunction and cardiac hypertrophy in mice. Free Radic Biol Med 2015;80: 84–92.
14. Tiniakos DG, Vo MB, Brunt EM. Nonalcoholic fatty liver disease: pathology and pathogenesis. Annu Rev Pathol 2010;5:145–171.
15. Postic C, Girard J. Contribution of de novo fatty acid synthesis to hepatic steatosis and insulin resistance: lessons from genetically engineered mice. J Clin Invest 2008;118:829–838.
16. Liu B, Chen Y, St. Clair DK. ROS and p53: a versatile partnership. Free Radic Biol Med 2008;44:1529–1535.
17. Maillet A, Pervaiz S. Redox regulation of p53, redox effectors regulated by p53: a subtle balance. Antioxid Redox Signal 2012;16:1285–1294.
18. Ryan MT, Hoogenraad HJ. Mitochondrial-nuclear communications. Annu Rev Biochem 2007;76:701–722.
19. Tae HJ, Zhang S, Kim KH. cAMP activation of CAAT enhancer-binding protein-beta gene expression and promoter I of acetyl-CoA carboxylase. J Biol Chem 1995;270:21487–21494.
20. Tae HJ, Luo X, Kim KH. Roles of CCAAT/enhancer-binding protein and its binding site on repression and derepression of acetyl-CoA carboxylase gene. J Biol Chem 1994;269:10475–10484.
21. Badman MK, Pissios P, Kennedy AR, Koukos G, Flier JS, Maratos-Flier E. Hepatic fibroblast growth factor 21 is regulated by PPARalpha and is a key mediator of hepatic lipid metabolism in ketotic states. Cell Metab 2007;5:426–437.
22. Kharitonenkov A, Larsen P. FGF21 reloaded: challenges of a rapidly growing field. Trends Endocrinol Metab 2011;22:81–86.
23. Liu J, Xu Y, Hu Y, Wang G. The role of fibroblast growth factor 21 in the pathogenesis of non-alcoholic fatty liver disease and implications for therapy. Metab Clin Exp 2015;64:380–390.
24. Hirosumi J, Tuncman G, Chang L, Görgün CZ, Uysal KT, Maeda K, et al. A central role for JNK in obesity and insulin resistance. Nature 2002;420:333–336.
25. Cao W, Collins QF, Becker TC, Robidoux J, Lupo EG, Xiong Y, et al. p38 Mitogen-activated protein kinase plays a stimulatory role in hepatic gluconeogenesis. J Biol Chem 2005;280:42731–42737.
26. Jeanson Y, Ribas F, Galinier A, Arnaud E, Ducos M, André M, et al. Lactate induces FGF21 expression in adipocytes through a p38-MAPK pathway. Biochem J 2016;473:685–692.
27. Vernia S, Cavanagh-Kyros J, Barrett T, Tournier C, Davis RJ. Fibroblast growth factor 21 mediates glycemic regulation by hepatic JNK. Cell Rep 2016;14:2273–2280.
28. Wente W, Efanov AM, Brenner M, Kharitonenkov A, Köster A, Sandusky GE, et al. Fibroblast growth factor-21 improves pancreatic beta-cell function and survival by activation of extracellular signal-regulated kinase 1/2 and Akt signaling pathways. Diabetes 2006;55: 2470–2478.
29. Porstmann T, Griffiths B, Chung YL, Delpuech O, Griffiths JR, Downward J, Schulze A. PKB/Akt induces transcription of enzymes involved in cholesterol and fatty acid biosynthesis via activation of SREBP. Oncogene 2005;24:6465–6481.
30. Wellen KE, Hotamisligil GS. Inflammation, stress, and diabetes. J Clin Invest 2005;115:1111–1119.
31. Kawauchi K, Araki K, Tobiume K, Tanaka N. p53 regulates glucose metabolism through an IKK-NF-kappaB pathway and inhibits cell transformation. Nat Cell Biol 2008;10:611–618.
32. Rahman SM, Schroeder-Gloeckler JM, Jansse RC, Jiang H, Qadri I, Maclean KN, Friedman JE. CCAAT/enhancing binding protein beta deletion in mice attenuates inflammation, endoplasmic reticulum stress, and lipid accumulation in diet-induced nonalcoholic steatohepatitis. Hepatology 2007;45:1108–1117.
33. Cai D, Yuan M, Frantz DF, Melendez PA, Hansen L, Lee J, Shoelson SE. Local and systemic insulin resistance resulting from hepatic activation of IKK-beta and NF-kappaB. Nat Med 2005;11:183–190.
34. Solinas G, Karin M. JNK1 and IKKbeta: molecular links between obesity and metabolic dysfunction. FASEB J 2010;24:2596–2611.
35. Schwabe RF, Brenner DA. Mechanisms of liver injury. I. TNF-alpha-induced liver injury: role of IKK, JNK, and ROS pathways. Am J Physiol Gastrointest Liver Physiol 2006;290:G583–G589.
36. Finkel T. Signal transduction by reactive oxygen species. J Cell Biol 2011;194:7–15.
37. Hamanaka RB, Chandel NS. Mitochondrial reactive oxygen species regulate cellular signaling and dictate biological outcomes. Trends Biochem Sci 2010;35:505–513.